ELSEVIER

Materials Science and Engineering A 425 (2006) 349–360

MATERIALS SCIENCE & ENGINEERING A

www.elsevier.com/locate/msea

Elastic and thermal expansion behavior of two-phase composites

Chin-Lung Hsieh, Wei-Hsing Tuan *

Department of Materials Science and Engineering, National Taiwan University, Taipei 106, Taiwan

Received 26 September 2005; received in revised form 21 March 2006; accepted 27 March 2006

Abstract

A first attempt has been made to propose a model to predict both the elastic constants and thermal expansion coefficient of two-phase composites. The model assumes that the two-phase composite is composed of many identical unit cells, and each unit cell is composed of a continuous matrix phase and an elongated particulate. The unit cell is further divided into several subunits; the two phases in each subunit are arranged either in series or in parallel. By inputting the basic information of each phase, the model could predict the upper and lower bounds of various elastic constants (e.g. elastic, shear and bulk moduli and Poisson's ratio) and thermal expansion coefficient of two-phase composites. Comparisons between the model predictions and available experimental measurements are carried out. There is an excellent match between the stimulated upper and lower bounds and experimental data over the entire composition range.

Keywords: Composites; Modeling; Elastic behavior; Thermal expansion

1. Introduction

The elastic and thermal properties of a monolithic material depend strongly on its bonding characteristics [1]. The performance of two-phase composites usually does not obey simple mixture rules [2], and therefore, it is critical to develop a model which could predict the elastic and thermal constants of composites. Without such a model, the design of composites with tailored elastic and thermal properties would be nearly impossible. Nevertheless, it is not practical to offer predictions of fixed property values for a certain composition. This is mainly due to the fact that the elastic constants and thermal expansion coefficient of a composite depend strongly on the shape and distribution of the second phase [3,4]. Attempting a prediction of the upper and lower bound values of a particular elastic or thermal property would seem to be more sensible; however, these two values need to be as close as possible for a useful and precise prediction.

Although a lengthy literature has now been developed to predict the elastic constants and thermal expansion coefficient of composites [3–27], a satisfactory separation between the upper and lower bound predictions is still lacking, especially for the Poisson's ratio [19]. Also, the existing modeling works for the elastic constants and thermal expansion coefficient are often carried out on different bases. It has been demonstrated that the thermal expansion coefficient of a composite is strongly dependent on the elastic properties of the phases within the composite [24–26]. The notion is logical since strains induced by temperature changes usually fall within the elastic range, and the expansion of one phase within a composite is governed by the rigidity of its neighboring phases. In the present study, a model which predicts both the elastic constants and thermal expansion coefficient of composites is developed. The validity of the model is evaluated against the measured experimental data.

2. Modeling

The following assumptions are made to derive the model for both elastic and thermal expansion constants. The two-phase composites are fully dense and their interfaces are strong. Therefore, it is not possible for the two components to separate at their

* Corresponding author. Tel.: +886 2 23659800; fax: +886 2 23634562.
E-mail address: tuan@ccms.ntu.edu.tw (W.-H. Tuan).

0921-5093/$ – see front matter © 2006 Elsevier B.V. All rights reserved.
doi:10.1016/j.msea.2006.03.073

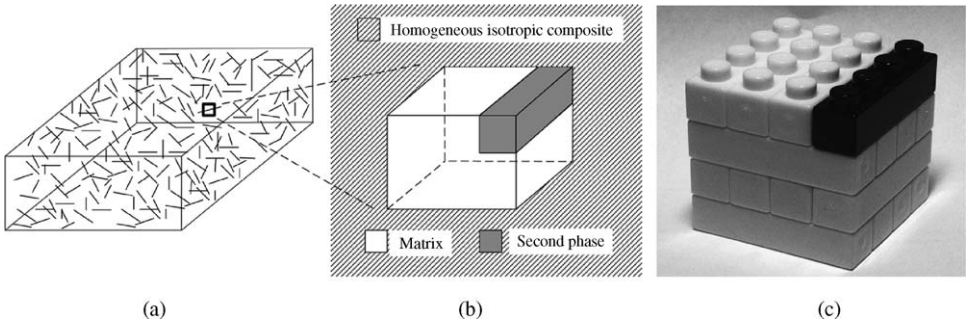

Fig. 1. (a) Schematic of a short fiber reinforced composite. The composite is composing of many identical (b) units. (c) One unit is demonstrated by using Logo blocks.

interfaces when the composite is loaded or heated. Additionally, only macro-composites are considered, namely, the scale of the reinforcement is large compared to that of the atom size or grain size so that composite properties can be modeled by continuum methods; and their properties are an appropriate average of those of the components.

2.1. Geometry

Most previous theoretical models on elastic constants treated the composite with isolated spherical particles [3,17]. Strictly speaking, these models should apply only for the composite with low second phase content. Though the models can always find some experimental data to support their feasibility over the entire composition range. However, one should note that the second phase particulates bound to touch each other above a threshold amount. Furthermore, the mechanical properties depend strongly on the shape of second phase. For example, the toughness of ceramic matrix composite is further enhanced by increasing the aspect ratio of second phase [28,29]. Therefore, one should pay attention to the composites with the microstructure as demonstrated in Fig. 1(a).

The composite shown in Fig. 1(a) can be visualized as a body composing of many unit cells as shown in Fig. 1(b) and (c). The geometry of one unit cell is shown in Fig. 2(A). The white phase in the matrix is a continuous phase. The gray phase is the second phase. The volume fraction of the second phase, V_p, can thus be related to its dimensions as

$$c = \frac{b}{a} = \left(\frac{1}{V_p}\right)^{1/2} - 1 \tag{1}$$

where c is the ratio of a to b.

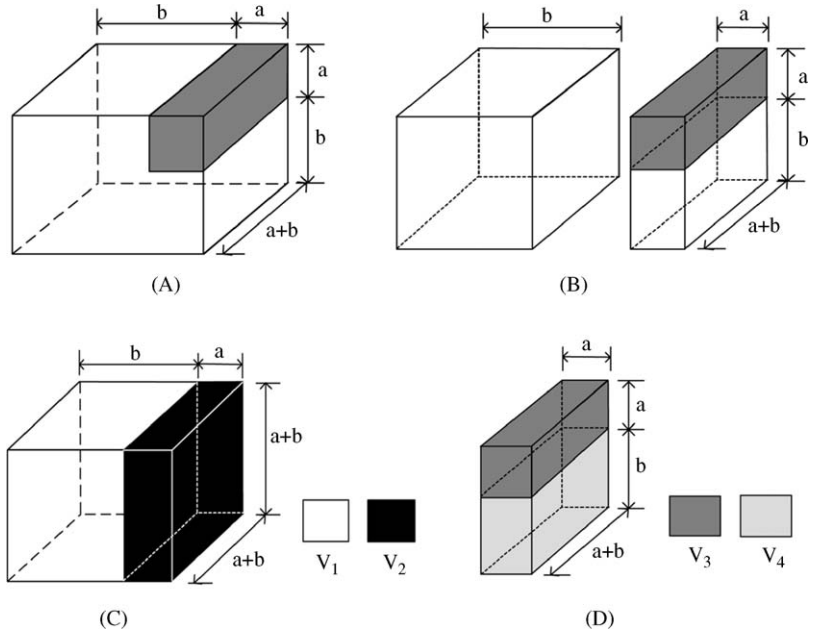

Fig. 2. (A) Dimensions of one unit cell and (B–D) the subunits. The volume fraction of each subunit is shown in Table 1.

Table 1
Volume fraction of the second phase in each subunit cell shown in Fig. 2

Sub-unit	vol.%
V_1 in Fig. 2(C)	$\frac{c}{c+1}$
V_2 in Fig. 2(C)	$\frac{1}{c+1}$
V_3 in Fig. 2(D)	$\frac{1}{c+1}$
V_4 in Fig. 2(D)	$\frac{c}{c+1}$

By adopting the methodology proposed by Ravichandran [17], each unit cell can be further divided into two sub-units as shown in Fig. 2(B). Within the sub-unit cell, the two phases are either in series or in parallel arrangement. The volume fraction of the second phase in each sub-unit can be found in Table 1.

2.2. Elastic constants of composites

As two phases in a composite are arranged in parallel, the elastic modulus of the composite, E_c, is [20,21]

$$E_{c,\text{parallel}} = E_a V_a + E_b V_b \tag{2}$$

For two in-series phases, the elastic modulus of the composite is [21,22]

$$\frac{1}{E_{c,\text{series}}} = \frac{V_a}{E_a} + \frac{V_b}{E_b} \tag{3}$$

The matrix and particulate in Fig. 2(C) and (D) are arranged in parallel and in series respectively as a load is applied in z-direction. For the elastic modulus of the composite shown in Fig. 2(D), by taking $V_a = V_4$, $V_b = V_3$, $E_a = E_m$, $E_b = E_p$, and the values from Table 1, the elastic modulus of the subunit is

$$E_{\text{Fig.2D}} = \frac{(1+c)E_m E_p}{cE_p + E_m} \tag{4}$$

For the subunit shown in Fig. 2(C), by taking $V_a = V_1$, $V_b = V_2$, $E_a = E_m$, $E_b = E_{\text{Fig.2D}}$, the elastic modulus of the composite is

$$E_c^l = \frac{(1+c+c^2)E_m E_p + cE_m^2}{(1+c)(cE_p + E_m)} \tag{5}$$

One should note that neither iso-strain nor iso-stress assumptions is realistic [5]. The traction at interface is not equilibrium under Fig. 2(C) condition; the interface could not remain intact under the Fig. 2(D) condition. The equality in Eq. (2) is true only when the Poisson's ratio of the two phases is the same. Nevertheless, the values predicted by Eqs. (2) and (3) are widely treated as the upper and lower bounds of the elastic modulus of two-phase composite [1–4]. To take the three-dimensional nature of stress and strain coupling into account, the elastic modulus of the composite with two phases arranged in series, is [21]

$$\frac{1}{E_{c,\text{series}}} = \frac{V_a}{E_a} + \frac{V_b}{E_b} - \frac{2((\nu_b/E_b) - (\nu_a/E_a))^2}{((1-\nu_b)/V_b E_b + (1-\nu_a)/V_a E_a)} \tag{6}$$

By taking $V_a = V_4$, $V_b = V_3$, $E_a = E_m$ and $E_b = E_p$, the elastic modulus of the subunit shown in Fig. 2(D) is

$$E_{\text{Fig.2D}} = \frac{E_m E_p (1+c)[c(1-\nu_p)E_m + (1-\nu_m)E_p]}{(cE_p + E_m)[(1-\nu_m)E_p + c(1-\nu_p)E_m] - 2c(\nu_m E_p - \nu_p E_m)^2} \tag{7}$$

For the subunit shown in Fig. 2(C), since $V_a = V_1$, $V_b = V_2$, $E_a = E_m$, $E_b = E_{\text{Fig.2D}}$ (Eq. (7)), the elastic modulus of the unit cell is

$$E_c^u = \frac{[(1+c+c^2)E_p E_m + cE_m^2][(1-\nu_m)E_p + c(1-\nu_p)E_m] - 2c^2 E_m(\nu_m E_p - \nu_p E_m)^2}{(1+c)\left\{(cE_p + E_m)[(1-\nu_m)E_p + c(1-\nu_p)E_m] - 2c(\nu_m E_p - \nu_p E_m)^2\right\}} \tag{8}$$

The Eqs. (5) and (8) are, respectively, the lower and upper bounds of the elastic modulus of the composite. The same methodology can be used to derive the expressions for shear modulus and bulk modulus.

As the two phases in a composite are arranged in parallel and the composite is under a load in z-direction, the Poisson's ratio of the composite is [17,19]

$$\nu_{c,\text{parallel}} = \nu_a V_a + \nu_b V_b \tag{9}$$

If the two phases are in-series arrangement, the Poisson's ratio of the composite is

$$\nu_{c,series} = \frac{\nu_a V_a E_b + \nu_b V_b E_a}{V_a E_b + V_b E_a} \tag{10}$$

For the subunit shown in Fig. 2(D), the matrix and particulate are in series, by taking $V_a = V_4$, $V_b = V_3$, $E_a = E_m$, $E_b = E_p$, $\nu_a = \nu_m$ and $\nu_b = \nu_p$ and the values from Table 1, the Poisson's ratio of the subunit is

$$\nu_{Fig.2D} = \frac{c\nu_m E_p + \nu_p E_m}{cE_p + E_m} \tag{11}$$

Then combines the subunit in Fig. 2(D) and a block of matrix to form the subunit as shown in Fig. 2(C), and taking $V_a = V_1$, $V_b = V_2$, $\nu_a = \nu_m$, $\nu_b = \nu_{Fig.2D}$ (Eq. (11)) and the corresponding values from Table 1, the Poisson's ratio of one unit cell is

$$\nu_c^u = \frac{c(1+c)\nu_m E_p + (c\nu_m + \nu_p)E_m}{(1+c)(cE_p + E_m)} \tag{12}$$

It assumes that there is no constraint for the elastic strain in lateral direction, the above equation thus corresponds to the upper value of the Poisson's ratio.

However, as long as the Poisson's ratio of two phases are different, the stress and strain are bound to couple to each other in order to maintain interface integrity. From Appendix A, the Poisson's ratio of the composite with two in-series phases is

$$\nu_{c,series} = \frac{[(1-\nu_b)E_a - (1-\nu_a)E_b]V_a + (\nu_a V_a E_b + \nu_b V_b E_a)X}{2(\nu_b E_a - \nu_a E_b)V_a + (V_a E_b + V_b E_a)X}$$

where X in the above equation is

$$X = \frac{(1-\nu_a)E_b V_b + (1-\nu_b)E_a V_a}{(\nu_a E_b - \nu_b E_a)V_b}$$

For the subunit shown in Fig. 2(D), the Poisson's ratio of the subunit is

$$\nu_{Fig.2D} = \frac{c[(1-\nu_p)E_m - (1-\nu_m)E_p](\nu_m E_p - \nu_p E_m) + (c\nu_m E_p + \nu_p E_m)[(1-\nu_m)E_p + c(1-\nu_p)E_m]}{(cE_p + E_m)[(1-\nu_m)E_p + c(1-\nu_p)E_m] - 2c(\nu_p E_m - \nu_m E_p)^2} \tag{13}$$

The Poisson's ratio of one unit cell is

$$\nu_c^l = \frac{\begin{array}{l}[c(1+c)\nu_m E_p + (\nu_p + c\nu_m)E_m][(1-\nu_m)E_p + c(1-\nu_p)E_m] \\ + c(\nu_m E_p - \nu_p E_m)[(1-\nu_p)E_m - (1-\nu_m)E_p - 2c\nu_m(\nu_m E_p + \nu_p E_m)]\end{array}}{(1+c)\left\{(cE_p + E_m)[(1-\nu_m)E_p + c(1-\nu_p)E_m] - 2c(\nu_m E_p - \nu_p E_m)^2\right\}} \tag{14}$$

The above equation describes the lower bound of the Poisson's ratio.

2.3. Thermal expansion coefficient of composites

For a composite containing two in-parallel phases, the thermal expansion of the composite is [26,27]

$$\alpha_{c,parallel} = \frac{\alpha_a E_a V_a + \alpha_b E_b V_b}{E_a V_a + E_b V_b} \tag{15}$$

As the two phases are in series arrangement in the composite, the thermal expansion coefficient of the composite is

$$\alpha_{c,series} = \alpha_a V_a + \alpha_b V_b \tag{16}$$

The strain of a monolith in z-direction is contributed by both an external stress (in z-direction), σ_z, and an external temperature change, ΔT, [1]

$$\varepsilon_z = \frac{\sigma_z}{E_c} + \alpha_c \Delta T \tag{17}$$

For a composite, the strain in z-direction of the composite is contributed by the strain from two in-series phases as

$$\varepsilon_z = \bar{\varepsilon}_z^a V_a + \bar{\varepsilon}_z^b V_b \tag{18}$$

From Eq. (A.9), the total strain in loading direction is

$$\varepsilon_z = \left[\frac{-2\nu_a}{E_a}\bar{\sigma}_x^a + \frac{1}{E_a}\bar{\sigma}_z^a + \alpha_a \Delta T\right] V_a + \left[\frac{-2\nu_b}{E_b}\bar{\sigma}_x^b + \frac{1}{E_b}\bar{\sigma}_z^b + \alpha_b \Delta T\right] V_b \tag{19}$$

As two phases are in-series arrangement under the load, the stress in each phase is the same, $\bar{\sigma}_z^a = \bar{\sigma}_z^b = \sigma_z$. Since there is no external stress in x- and y-directions, from Eq. (A.6),

$$\bar{\sigma}_x^b = -\left(\frac{V_a}{V_b}\right)\bar{\sigma}_x^a \tag{20}$$

By knowing the above relationship and rearranging Eq. (19), the following equation is obtained,

$$[\alpha_c - \alpha_a V_a - \alpha_b V_b]\Delta T = \bar{\sigma}_x^b\left[\frac{2\nu_a}{E_a} - \frac{2\nu_b}{E_b}\right]V_b + \sigma_z\left[\frac{V_a}{E_a} + \frac{V_b}{E_b} - \frac{1}{E_c}\right] \tag{21}$$

Assuming the interface remains in its perfect bonding, the lateral strain in each phase is the same, $\bar{\varepsilon}_x^a = \bar{\varepsilon}_x^b$. From Eqs. (A.10) and (21) can be expressed as

$$\frac{1-\nu_a}{E_a}\bar{\sigma}_x^a - \frac{\nu_a}{E_a}\bar{\sigma}_z^a + \alpha_a\Delta T = \frac{1-\nu_b}{E_b}\bar{\sigma}_x^b - \frac{\nu_b}{E_b}\bar{\sigma}_z^b + \alpha_b\Delta T \tag{22}$$

since $\bar{\sigma}_z^a = \bar{\sigma}_z^b = \sigma_z$,

$$(\alpha_a - \alpha_b)\Delta T = \bar{\sigma}_x^b\left[\frac{1-\nu_a}{E_a}\frac{V_b}{V_a} + \frac{1-\nu_b}{E_b}\right] + \sigma_z\left[\frac{\nu_a}{E_a} - \frac{\nu_b}{E_b}\right] \tag{23}$$

By comparing Eqs. (21) and (23), the following equation can be obtained,

$$\alpha_{c,\text{series}} = \alpha_a V_a + \alpha_b V_b + (\alpha_a - \alpha_b) \times \frac{2[(\nu_a/E_a) - (\nu_b/E_b)]}{(1-\nu_a)/E_a V_a + (1-\nu_b)/E_b V_b} \tag{24}$$

For the two phases in the subunit shown in Fig. 2(D), by taking $V_a = V_4$, $V_b = V_3$, $\alpha_a = \alpha_m$, $\alpha_b = \alpha_p$ and the corresponding values shown in Table 1, then using Eq. (16), the thermal expansion of the subunit is

$$\alpha_{\text{Fig.2D}} = \frac{c\alpha_m + \alpha_p}{c+1} \tag{25}$$

Then, for the unit shown in Fig. 2(C), by taking $V_a = V_1$, $V_b = V_2$, $E_a = E_m$, $E_b = E_{\text{Fig.2D}}$ (Eq. (4)), $\alpha_a = \alpha_m$, $\alpha_b = \alpha_{\text{Fig.2D}}$ (Eq. (25)) and using Eq. (15), the thermal expansion coefficient of one unit cell is

$$\alpha_c^l = \frac{(c\alpha_m + \alpha_p)E_m E_p + c\alpha_m E_m(cE_p + E_m)}{(c+1)E_m E_p + cE_m(cE_p + E_m)} \tag{26}$$

The above equation corresponds to the lower bound of the thermal expansion coefficient.

For the subunit shown in Fig. 2(D), the two phases are in series arrangement, by taking $V_a = V_4$, $V_b = V_3$, $\alpha_a = \alpha_m$, $\alpha_b = \alpha_p$, and insert the above equation into Eq. (24), the following equation is derived,

$$\alpha_{\text{Fig.2D}} = \frac{1}{c+1}\left[\frac{(c\alpha_m + \alpha_p)[(1-\nu_m)E_p + c(1-\nu_p)E_m] + 2c(\alpha_m - \alpha_p)(\nu_m E_p - \nu_p E_m)}{(1-\nu_m)E_p + c(1-\nu_p)E_m}\right] \tag{27}$$

For the unit cell shown in Fig. 2(C), by taking $V_a = V_1$, $V_b = V_2$, $\alpha_a = \alpha_m$, $E_a = E_m$, $\alpha_b = \alpha_{\text{Fig.2D}}$ (Eq. (27)), $E_b = E_{\text{Fig.2D}}$ (Eq. (7)) and using Eq. (15), the following relationship is obtained,

$$\alpha_c^u = \frac{A + c\alpha_m E_m}{B + cE_m} \tag{28}$$

where A and B in the above equation are as following,

$$A = \frac{E_p E_m\left\{(c\alpha_m + \alpha_p)[(1-\nu_m)E_p + c(1-\nu_p)E_m] + 2c(\alpha_m - \alpha_p)(\nu_m E_p - \nu_p E_m)\right\}}{(E_m + cE_p)[(1-\nu_m)E_p + c(1-\nu_p)E_m] - 2c(\nu_m E_p - \nu_p E_m)^2} \tag{29}$$

$$B = \frac{(1+c)E_p E_m[(1-\nu_m)E_p + c(1-\nu_p)E_m]}{(E_m + cE_p)[(1-\nu_m)E_p + c(1-\nu_p)E_m] - 2c(\nu_m E_p - \nu_p E_m)^2} \tag{30}$$

The Eq. (28) is the upper bound for the thermal expansion coefficient.

3. Comparison

3.1. Elastic constants

Figs. 3–5 show the comparison between the model predictions and experimental data [17,30–38]. The basic properties of each phase in the composites are shown in Table 2. Despite the elastic moduli ratio, E_p/E_m, varies in a wide range from 3.2 (for Co–WC composites) to 21 (for epoxy-glass fiber composites), the upper and lower bounds proposed in the present study covers most of the experimental data.

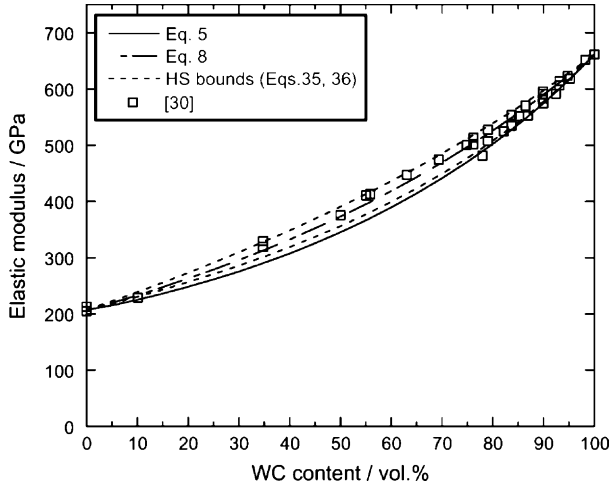

Fig. 3. Elastic modulus of Co–WC composites as function of WC content.

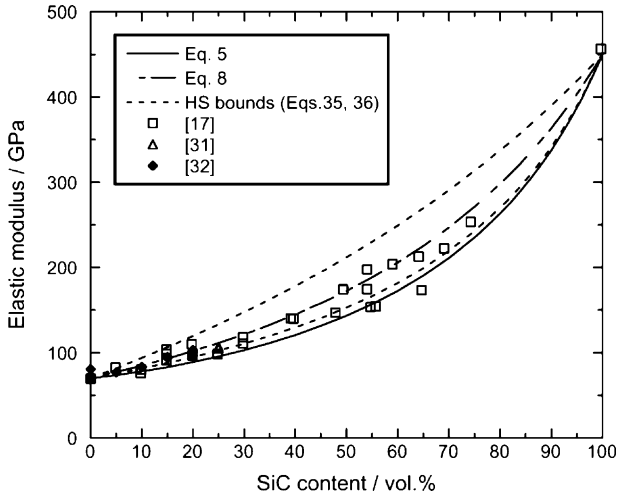

Fig. 4. Elastic modulus of Al–SiC composites as function of SiC content.

Table 2
Elastic moduli, Poisson's ratio and thermal expansion coefficient of the matrix and second phase for the composites collected in the present study

Systems (matrix-2nd phase)	E_m (GPa)	E_p (GPa)	E_p/E_m	ν_m	ν_p	ν_p/ν_m	α_m (ppm °C^{-1})	α_p (ppm °C^{-1})	α_m/α_p
Co–WC [30]	207	661	3.2	0.31	0.19	0.61	14	5.2	2.7
Al–SiC [17,31,32,39]	70	450	6.4	0.39	0.22	0.56	22	5.0	4.4
Epoxy–glass fiber [30,33–37,40]	3.5	73	21	0.35	0.22	0.63	–	–	–
Cu–diamond [44,45]	124	1000	8.1	0.34	0.20	0.59	19	2.2	8.6

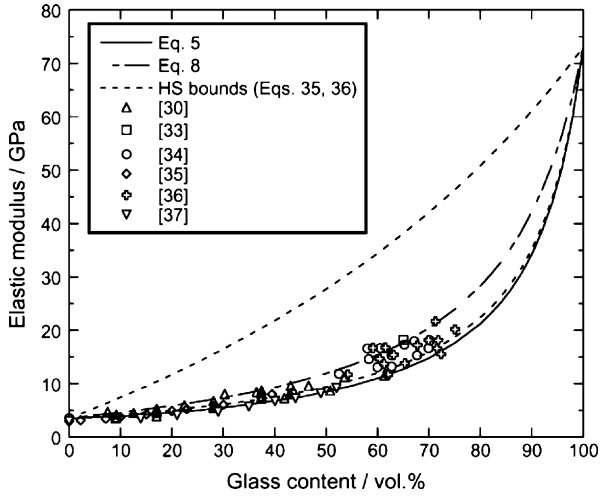

Fig. 5. Elastic modulus of epoxy–glass fiber composites as function of glass fiber content.

The Hashin and Shtrikman (H–S) bounds are also shown for comparison. The H–S model offers predictions for bulk and shear moduli as [13]

$$K_c^l = K_m + \frac{V_p}{1/(K_p - K_m) + 3V_m/(3K_m + 4G_m)} \tag{31}$$

$$K_c^u = K_p + \frac{V_m}{1/(K_m - K_p) + 3V_p/(3K_p + 4G_m)} \tag{32}$$

$$G_c^l = G_m + \frac{V_p}{1/(G_p - G_m) + 6(K_m + 2G_m)V_m/5G_m(3K_m + 4G_m)} \tag{33}$$

$$G_c^u = G_p + \frac{V_m}{1/(G_m - G_p) + 6(K_p + 2G_p)V_p/5G_p(3K_p + 4G_p)} \tag{34}$$

The upper and lower bounds on the elastic modulus are derived by using the following equation as

$$E_c^l = \frac{9K_c^l G_c^l}{3K_c^l + G_c^l} \tag{35}$$

$$E_c^u = \frac{9K_c^u G_c^u}{3K_c^u + G_c^u} \tag{36}$$

The H–S model was chosen for its wide popularity. Its popularity is based on the fact that the model offers coverage over the experimental data; furthermore, the separation between the upper and lower bounds is relatively narrow.

The modulus ratio, E_p/E_m, of the two phases in the composites shown in Figs. 3 and 4 is smaller than 10. For these composites, the upper and lower bounds proposed in the present study is close to the H–S bounds. However, as the moduli ratio, E_p/E_m, is larger than 20, Fig. 5, the bounds proposed in the present study are relatively closer to each other. It demonstrates that the model proposed in the present study can also offer prediction on the elastic modulus of composites. The model has also been applied to the comparison with the bulk and shear modulus. The match between theoretical predictions and experimental data can also be found. The improved correlation between the predictions and experimental data may result from the geometry of the model used in the present study.

Figs. 6–8 show the experimental data on the Poisson's ratio of several composites [17,37,39,40]. Though exhaustive search has been conducted, it was a surprise to the present authors that the sparse of the available data. It implies that the investigation on Poisson's ratio has attracted relatively little attention.

The basic properties of each phase in these composites are also shown in Table 2. The model predictions proposed in the present study cover most the experimental data. One may note that the separation between the upper and lower bounds shows strong dependence on E_p/E_m, less dependence on ν_p/ν_m. One can also note that the separation between the upper and lower bounds increases significantly with the increase of E_p/E_m.

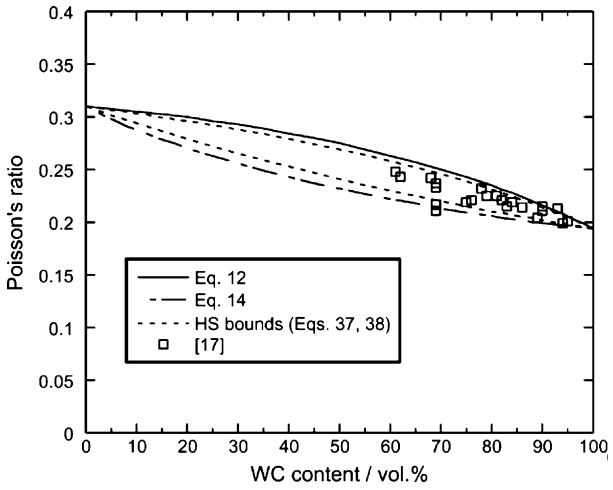

Fig. 6. Poisson's ratio of Co–WC composites as function of WC content.

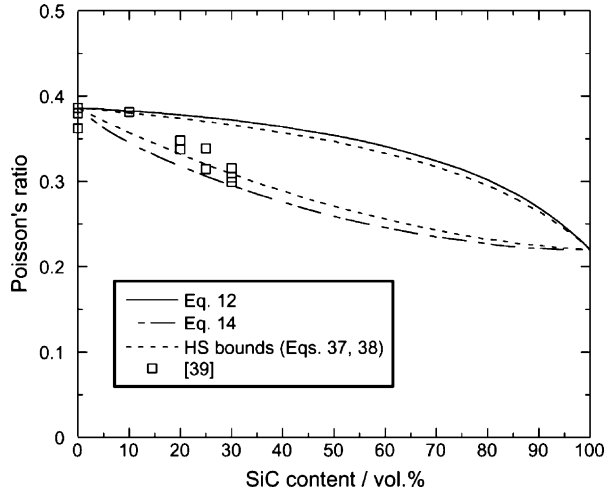

Fig. 7. Poisson's ratio of Al–SiC composites as function of SiC content.

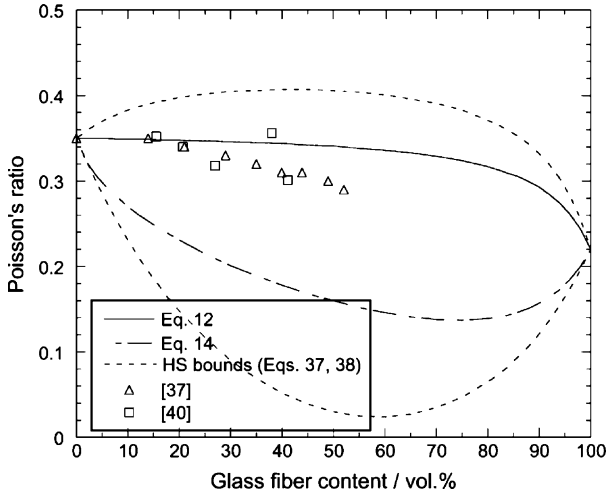

Fig. 8. Poisson's ratio of epoxy–glass fiber composites as function of glass fiber content.

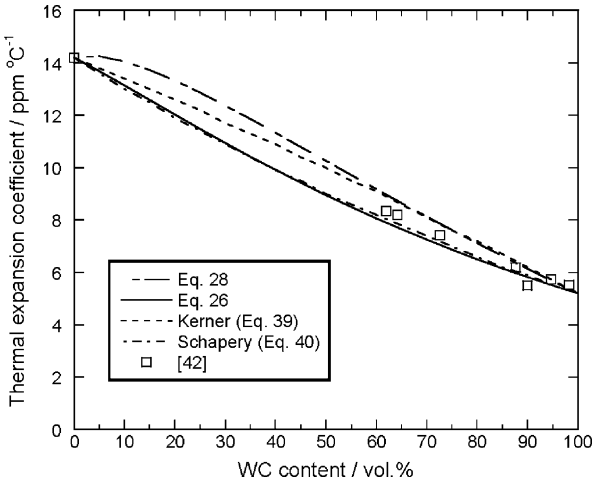

Fig. 9. Thermal expansion coefficient of Co–WC composites as function of WC content.

The bounds predicted by using the H–S model are also shown in the figures. The Poisson's ratio of the composites was calculated by using the bulk and shear moduli as following [18,41].

$$\nu_c^l = \frac{3K_c^l - 2G_c^u}{6K_c^l + 2G_c^u} \tag{37}$$

$$\nu_c^u = \frac{3K_c^u - 2G_c^l}{6K_c^u + 2G_c^l} \tag{38}$$

As the E_p/E_m ratio is smaller than 10, the upper and lower bounds on Poisson's ratio are very close to those of the H–S model, Figs. 6 and 7. Furthermore, the upper and lower bounds proposed in the present study cover more experimental data than those predicted by the H–S models. As the elastic modulus ratio is larger than 20 (Fig. 8), the bounds proposed in the present study is closer than those from H–S model. It demonstrates the improved prediction on the Poisson's ratio by applying the present model. In the present study, the stress-strain coupling is taken into account. Furthermore, since the Poisson's ratio is derived from the shear and bulk moduli (Eqs. (37) and (38)); better description on the moduli results in improved prediction on Poisson's ratio. However, the match between the prediction and experimental measurements is still disappointing. The present authors would think that the stress–strain coupling in three dimensions plays an important role on the Poisson's ratio. Though the approach proposed by Owen and Koller [21] has been adopted in this study to solve the problem, the predictions on the Poisson's ratio are not satisfactory. It suggests that a more comprehensive solution on Poisson's ratio is still needed.

3.2. Thermal expansion coefficient

The experimental data on the thermal expansion coefficient of the Co–WC, Al–SiC and Cu–diamond composites are shown in Figs. 9–11 [42–45]. The basic properties of each phase in the composites are shown in Table 2. Though the thermal expansion coefficient ratio, α_m/α_p, for the composites varies in a large range, from 1.9 to 8.6, the match between the model predictions and experimental data has been found.

After comparing various previous models [22–27] for thermal expansion coefficient, Kerner and Schapery model predictions offer the largest and lowest values for the experimental data. Therefore, the predictions proposed by Kerner (Eq. (39)) and Schapery (Eq. (40)) are also shown in the figures. The Kerner and Schapery models are shown respectively below [24,25],

$$\alpha_c = \alpha_m V_m + \alpha_p V_p + V_m V_p(\alpha_p - \alpha_m) \times \frac{K_p - K_m}{V_m K_m + V_p K_p + (3K_m K_p/4G_m)} \tag{39}$$

$$\alpha_c = \alpha_p + (\alpha_m - \alpha_p)\frac{(1/K_c) - (1/K_p)}{(1/K_m) - (1/K_p)} \tag{40}$$

The upper and lower bounds proposed in the present study and Kerner–Schapery bounds show coverage on the experimental data. However, the bounds proposed in the present study offer a slightly better coverage on the experimental data. It demonstrates that the thermal expansion behavior of composite depends strongly on its elastic constants. Precise description on the elastic moduli ensures improved prediction on the thermal expansion coefficient.

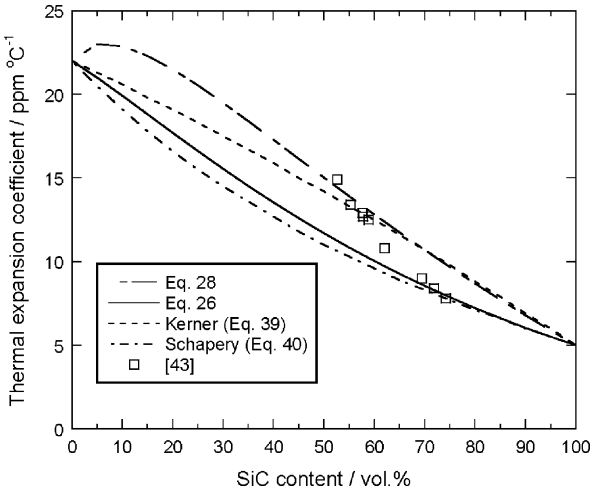

Fig. 10. Thermal expansion coefficient of Al–SiC composites as function of SiC content.

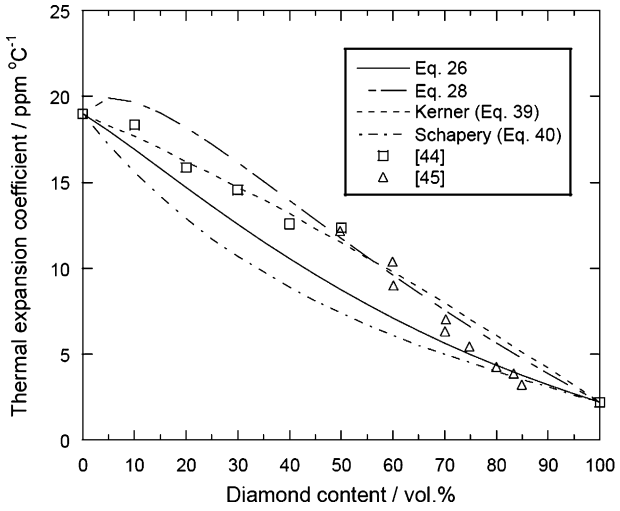

Fig. 11. Thermal expansion coefficient of Cu–diamond composites as function of diamond content.

4. Conclusions

A modified unit-cell model is proposed in the present study. The model offers a pair of upper and lower bounds on the elastic constants and thermal expansion coefficient. The predictions cover a number of experimental data sets over entire composition range. The model predictions proposed in the present study are also compared with other theoretical models. Improved predictions on the experimental data are observed.

Acknowledgment

The present work was supported by the National Science Council, R.O.C. through Contract No. NSC93-2216-E002-016.

Appendix A

Assuming that there are two in-series phases, A and B, in a composite, no displacement or slip takes place at the interface as an external load and/or a temperature change are applied onto the composite. The strain induced by the elastic and thermal stresses, Fig. 4(c), is as following [1]:

$$\varepsilon_z = \frac{\sigma_z}{E_c} + \alpha_c \Delta T \tag{A.1}$$

For each phase, the strain in A or B is

$$\bar{\varepsilon}_z^{a,b} = \frac{\bar{\sigma}_z^{a,b}}{E_{a.b}} + \alpha_{a,b}\Delta T \tag{A.2}$$

Assuming that the stress is in the z-direction, the stress is

$$\sigma_z = E_c(\varepsilon_z - \alpha_c \Delta T) \tag{A.3}$$

The stress in each phase A or B can be expressed as,

$$\bar{\sigma}_z^{a,b} = E_{a,b}(\bar{\varepsilon}_z^{a,b} - \alpha_{a,b}\Delta T) \tag{A.4}$$

By taking the volume fraction of A and B into account as

$$\sigma_z = \bar{\sigma}_z^a V_a + \bar{\sigma}_z^b V_b \tag{A.5}$$

$$\sigma_{x,y} = \bar{\sigma}_{x,y}^a V_a + \bar{\sigma}_{x,y}^b V_b \tag{A.6}$$

$$\varepsilon_z = \bar{\varepsilon}_z^a V_a + \bar{\varepsilon}_z^b V_b + \alpha_c \Delta T \tag{A.7}$$

$$\varepsilon_{x,y} = \bar{\varepsilon}_{x,y}^a V_a + \bar{\varepsilon}_{x,y}^b V_b + \alpha_c \Delta T \tag{A.8}$$

The Poisson's ratio effect is also needed to be considered, namely the lateral strain is also considered, the strain in each direction is

$$\bar{\varepsilon}_z^{a,b} = \frac{-2\nu_{a,b}}{E_{a,b}}\bar{\sigma}_x^{a,b} + \frac{1}{E_{a,b}}\bar{\sigma}_z^{a,b} + \alpha_{a,b}\Delta T \tag{A.9}$$

$$\bar{\varepsilon}_x^{a,b} = \frac{1-\nu_{a,b}}{E_{a,b}}\bar{\sigma}_x^{a,b} - \frac{\nu_{a,b}}{E_{a,b}}\bar{\sigma}_z^{a,b} + \alpha_{a,b}\Delta T \tag{A.10}$$

Since the Poisson's ratio is the ratio of the strain in x- (or y-) direction to that of z-direction as

$$\nu = -\frac{\varepsilon_x}{\varepsilon_z} \tag{A.11}$$

The expressions for ε_x and ε_z can be found from Eqs. (A.5)–(A.10). For a composite with two in-series phase at constant temperature condition ($\Delta T = 0$), the Eq. (A.11) can then transform into

$$\nu_{c,\text{series}} = -\frac{[((1-\nu_a)/E_a)\bar{\sigma}_x^a - (\nu_a/E_a)\bar{\sigma}_z^a]V_a + [((1-\nu_b)/E_b)\bar{\sigma}_x^b - (\nu_b/E_b)\bar{\sigma}_z^b]V_b}{[(-2\nu_a/E_a)\bar{\sigma}_x^a + (1/E_a)\bar{\sigma}_z^a]V_a + [(-2\nu_b/E_b)\bar{\sigma}_x^b + (1/E_b)\bar{\sigma}_z^b]V_b} \tag{A.12}$$

In order to maintain interface integrity, the strain along the interface of two in-series phases is the same. From Eq. (A.10),

$$\frac{1-\nu_a}{E_a}\bar{\sigma}_x^a - \frac{\nu_a}{E_a}\bar{\sigma}_z^a = \frac{1-\nu_b}{E_b}\bar{\sigma}_x^b - \frac{\nu_b}{E_b}\bar{\sigma}_z^b \tag{A.13}$$

The stress in x-direction is zero, from Eq. (A.6),

$$\bar{\sigma}_x^b = -\left(\frac{V_a}{V_b}\right)\bar{\sigma}_x^a \tag{A.14}$$

By knowing Eq. (A.14), the Eq. (A.13) can be changed into

$$\bar{\sigma}_z^a = \bar{\sigma}_z^b = \frac{(1-\nu_a)E_bV_b + (1-\nu_b)E_aV_a}{(\nu_aE_b - \nu_bE_a)V_b}\bar{\sigma}_x^a \tag{A.15}$$

Since the expressions for the stress in x- and z-directions are known, the Poisson's ratio of two in-series phases is

$$\nu_{c,\text{series}} = \frac{[(1-\nu_b)E_a - (1-\nu_a)E_b]V_a + (\nu_aV_aE_b + \nu_bV_bE_a)X}{2(\nu_bE_a - \nu_aE_b)V_a + (V_aE_b + V_bE_a)X} \tag{A.16}$$

where X in the above equation is as following:

$$X = \frac{(1-\nu_a)E_bV_b + (1-\nu_b)E_aV_a}{(\nu_aE_b - \nu_bE_a)V_b} \tag{A.17}$$

References

[1] M.F. Ashby, D.R.H. Jones, Engineering Materials. I. An Introduction to their Properties and Applications, 1st ed., Pergamon Press, Oxford, 1980.
[2] Z. Hashin, J. Appl. Mech. 50 (1983) 481.
[3] Z. Fan, P. Tsakiropoulos, A.P. Miodownik, Mater. Sci. Eng. 8 (1992) 922.
[4] D.K. Hale, J. Mater. Sci. 11 (1976) 2105.
[5] R. Hill, J. Mech. Phys. Solids 11 (1963) 357.
[6] J.P. Watt, G.F. Davies, R.J. O'Connell, Rev. Geophys. Space Phys. 14 (1976) 541.
[7] M.F. Ashby, Acta Metal Mater. 40 (1993) 1313.
[8] J.P. Matt, Phys. Chem. Min. 15 (1988) 579.
[9] J.C. Halpin, J.L. Kardos, Ploym. Eng. Sci. 16 (1976) 344.
[10] T.T. Wu, J. Appl. Mech. 32 (1965) 211.
[11] T.T. Wu, Int. J. Solids Struct. 2 (1966) 1.
[12] B. Paul, Trans. AIME 218 (1960) 36.
[13] Z. Hashin, S. Shtrinkman, J. Mech. Phys. Solids 11 (1963) 127.
[14] R. Hill, J. Mech. Phys. Solids 11 (1963) 357.
[15] C.M. Salerno, J.P. Watt, J. Appl. Phys. 60 (1986) 1618.
[16] L.J. Walpole, J. Mech. Phys. Solids 14 (1966) 155.
[17] K.S. Ravichandran, J. Am. Ceram. Soc. 77 (1994) 1178.
[18] R.W. Zimmerman, Mech. Res. Commun. 19 (1992) 563.
[19] C.L. Hsieh, W.H. Tuan, Mater. Sci. Eng. A 396 (2005) 202.
[20] W. Voigt, Ann. Phys. 38 (1928) 573.
[21] A.J. Owen, I. Koller, Polymer 37 (1996) 527.
[22] A. Ruess, Z. Angrew, Math. Mech. 9 (1929) 49.
[23] P.S. Turner, J. Res. Natl. Bureau Stand. 37 (1946) 239.
[24] E.H. Kerner, Proc. Phys. Soc. 69 (1956) 808.
[25] R.A. Schapery, J. Comp. Mater. 2 (1968) 380.
[26] B.W. Rosen, Z. Hashin, Int. J. Eng. Sci. 8 (1970) 157.
[27] S. Elomari, M.D. Skibo, A. Sundarrajan, H. Richards, Comp. Sci. Technol. 58 (1998) 369.
[28] K.T. Faber, A.G. Evans, Acta Metall. 31 (1983) 565.
[29] C.L. Hsieh, W.H. Tuan, T.T. Wu, J. Eur. Ceram. Soc. 24 (2004) 3789.
[30] Z. Fan, P. Tsakiropoulos, A.P. Miodownik, Mater. Sci. Eng. 8 (1992) 922.
[31] G.P. Mott, K. Liaw, Metall. Trans. A 19A (1988) 2233.
[32] M.R. Orrhede, K. Tolani, Res. Nondestr. Eval. 8 (1996) 23.
[33] I. Ivanow, A. Tabiei, Comp. Struct. 54 (2001) 489.
[34] H.Z. Shan, T.W. Chou, Comp. Sci. Technol. 53 (1995) 383.
[35] L. Banks-Sills, V. Leiderman, D. Fang, Composites Part B 28B (1997) 465.
[36] G.R. Liu, Comp. Struct. 40 (1998) 313.
[37] P.R. Marur, Acta Mater. 52 (2000) 1263.
[38] M. Krumova, C. Klingshirn, F. Haupert, K. Friendrich, Comp. Sci. Technol. 61 (2001) 557.
[39] P.K. Liaw, R.E. Shannon, W.G. Vlark, J.W.C. Harrigan, J.H. Jeong, D.K. Hsu, Mater. Chem. Phys. 39 (1995) 220.
[40] O.I. Okoli, G.F. Smith, Comp. Struct. 48 (2000) 157.
[41] C.L. Hsieh, W.H. Tuan, Mater. Sci. Eng. A 396 (2005) 202.
[42] N. Chawla, B.V. Patel, M. Koopman, K.K. Chawla, R. Saha, B.R. Patterson, E.R. Fuller, A. Langer, Mater. Charact. 49 (2003) 395.
[43] R. Arpon, J.M. Molina, R.A. Saravanan, C. Garcya-Cordovilla, E. Louis, J. Narciso, Acta Mater. 51 (2003) 3145.
[44] Q. Sun, O.T. Inal, Mater. Sci. Eng. B 41 (1996) 261.
[45] K. Yoshida, H. Morigami, Microelect. Reliab. 44 (2004) 303.